Evaporation and capillary coupling across vertical textural contrasts in porous media

Peter Lehmann* and Dani Or†
Department of Environmental Sciences, ETH Zürich, Universitätstrasse 16, 8092 Zurich, Switzerland
(Received 18 March 2009; published 27 October 2009)

High and nearly constant evaporation rates from initially saturated porous media are sustained by capillary-driven flow from receding drying front below the evaporating surface. The spatial extent of continuous liquid pathways in homogeneous porous medium is defined by its hydraulically connected pore size distribution. We consider here evaporative losses from porous media consisting of two hydraulically coupled dissimilar domains each with own pore and particle size distributions separated by sharp vertical textural contrast. Evaporation experiments from texturally dissimilar media were monitored using neutron transmission and dye pattern imaging to quantify water distribution and drying front dynamics. Drying front invades exclusively coarse-textured domain while fine-textured domain remains saturated and its surface continuously coupled with the atmosphere. Results show that evaporation from fine-textured surface was supplied by liquid flow from adjacent coarse domain driven by capillary pressure differences between the porous media. A first characteristic length defining limiting drying front depth during which fine sand region remains saturated is deduced from difference in air-entry pressures of the two porous media. A second characteristic length defining the end of high evaporation rate includes the extent of continuous liquid films pinned in the crevices of the pore space and between particle contacts in the fine medium. We established numerically the lateral extent of evaporation-induced hydraulic coupling that is limited by viscous losses and gravity. For certain combinations of soil types the lateral extent of hydraulic coupling may exceed distances of 10 m. Results suggest that evaporative water losses from heterogeneous and coupled system are larger compared with uncoupled or homogenized equivalent systems.

DOI: 10.1103/PhysRevE.80.046318 PACS number(s): 47.56.+r, 68.05.−n, 64.70.F−, 95.75.Mn

I. INTRODUCTION

Evaporation rate from porous media is determined by complex interactions between internal transport mechanisms, media properties, and external boundary conditions. Early stages of evaporation from initially saturated porous media are often marked by high and relatively constant drying rate (stage 1) and formation of a receding drying front. Capillary flow along hydraulically connected pathways [1,2] through partially saturated zone above the drying front denoted as "film region" [3] sustains high evaporation rates. The extent of the film region is determined by balance between flow inducing capillary gradients and counteracting gravitational forces and viscous dissipation. These forces are not determined by representative pore size only as previously assumed [4,5] but by differences in hydraulically connected pore size distributions. A capillary pressure gradient spanned by differences in pore size distributions drives liquid flow from large pores to supply water evaporating from small pores at the surface [6]. The importance of capillary-driven liquid flow for drying processes was discussed in previous studies denoting this flow mechanism as "capillary pumping" [7], "capillary transfer" [8], or "counterflow" [9]. In this study we extend the concept to consider internal exchanges and evaporation from "capillary coupled" or hydraulically coupled porous domains highlighting the potential for heterogeneity-enhanced evaporative losses. Lehmann *et al.* [10] demonstrated that the spatial extent of capillary-flow region between a receding drying front and evaporating surface could be deduced directly from capillary pressure-saturation relationship for the porous medium. Additionally, capillary pressure at the drying front remains at air-entry value whereas capillary pressure at the surface gradually becomes more negative pulling water upward (against gravity) from the drying front along liquid structures remaining in connected pores and crevices. When gravity exceeds maximum capillary pressure difference between the drying front (air-entry value) and the surface, water recedes from the surface and drying rate dropped to vapor diffusion controlled stage 2. In fine-textured porous media viscous resistance introduces an additional constraint to gravity reducing the extent of film region. Additionally, for high drying rates, evaporation flux can be limited by coupling between evaporating surface and air boundary layer above [11–13]. However, surface-air coupling does not affect the film region extent and associated reduction in drying rate due to this coupling effect is considered as stage 1 as well.

Evaporation from initially saturated porous system containing abrupt vertical textural contrasts introduces an additional form of hydraulic coupling and mass exchange between the texturally different domains. Experimental evidence of structural and textural effects on drying front patterns is shown in Fig. 1. While drying patterns and rates of the two homogeneous sand columns shown in Fig. 1 could be understood in terms of the width of the pore size distribution [10], the drying front pattern in the column with interacting fine and coarse sand domains cannot be deduced from drying front behavior in the homogeneous columns. The drying front propagates exclusively in the coarse sand domain while the fine sand domain remains water saturated.

*peter.lehmann@env.ethz.ch
†dani.or@env.ethz.ch

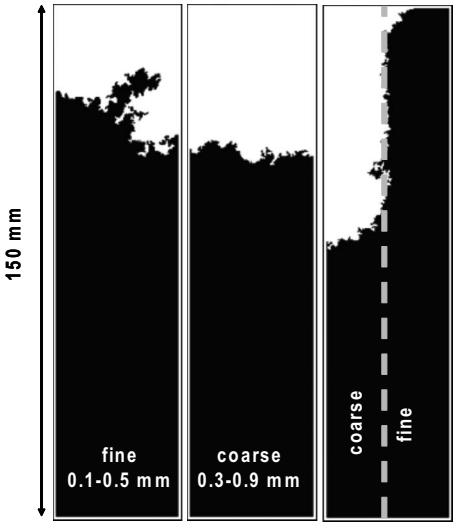

FIG. 1. Drying of porous media affected by texture and coupling. Three initially saturated sand filled Hele-Shaw cells of 10 mm thickness are separated by glass walls. The distribution of water saturated (black) and partially air-filled region (white) was deduced from the distribution of blue dye. Two cells (on left) were filled homogeneously with one type of sand material (grain size range is indicated) and the drying front penetrates in both media with similar velocities during stage 1. In the third column (right) fine and coarse sands are hydraulically coupled and the air phase enters preferentially the coarse material with completely saturated fine sand. The gray vertical dashed line indicates the position of the material interface.

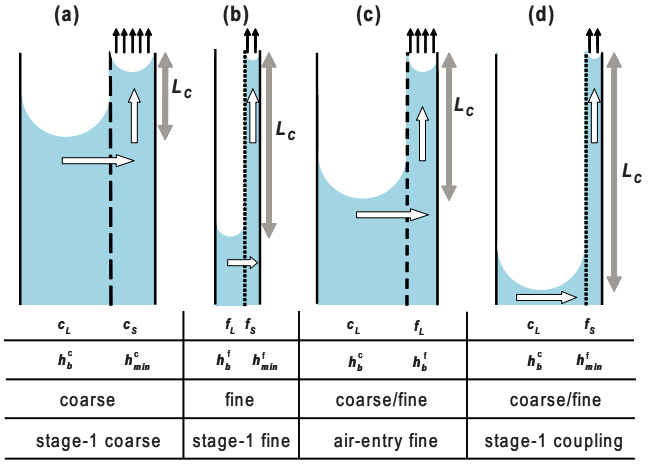

FIG. 2. (Color online) Characteristic length (L_C) and capillary coupling between large (index L) and small (S) capillaries and coarse (c) and fine (f) materials. The capillaries represent effective capillary pressures defining air-entry value h_b and value close to residual value $h_{\min}$ driving liquid flow (white arrows) to replace water evaporated from the surface (black arrows). The dashed vertical lines denote the positions of the material interface. In (a) and (b) the characteristic lengths L_C for homogeneous coarse and fine materials are shown. (c) defines the depth of the meniscus (front depth) in the coarse just before air can enter the fine domain. (d) shows the end of stage 1 with flow from the drying front in the coarse to the partially saturated fine-textured surface. In this conceptual figure, viscous effects are neglected and the characteristic length equals the gravitational length L_G.

The objective of this study is to quantify and predict impact of vertical textural contrast on stage-1 evaporative drying (always directed against gravity). The process is conceptualized by extending a simple model originally proposed by Krischer [14] that considers hydraulically interacting pairs of capillaries with different radii inducing capillary flow from the large to the small capillary having a pinned meniscus evaporating at its top. The extension of the conceptual picture to hydraulically interacting domains in a porous medium with abrupt textural transitions is relatively straightforward.

The consequences of such coupling give rise to several interesting phenomena with potentially important hydrologic and engineering applications for evaporation from heterogeneous porous media. In this study we extended the concept of evaporation characteristic length of Lehmann *et al.* [10] to heterogeneous porous media, considering, in a first step, simple heterogeneities such as abrupt textural changes when two materials are arranged in parallel. The specific objectives were to quantify effects of vertical textural discontinuities on (1) drying front displacement patterns, (2) duration and maximum front depth of stage-1 evaporation, and (3) total evaporative water losses as compared with homogeneous porous medium under similar conditions.

II. THEORETICAL CONSIDERATIONS

The duration of the stage-1 evaporation and the maximum drying front depth before capillary liquid connections are interrupted is determined by a characteristic length that depends on the driving capillary forces and counteracting gravitational and viscous effects. At the microscopic scale, the characteristic length of homogeneous and heterogeneous materials is introduced by representing the porous medium by a pair of equivalent capillaries with well defined air-entry pressures. At the macroscale, the effect of hydraulic coupling is deduced from relationship between capillary pressure head h, liquid saturation θ, and hydraulic conductivity K of the coupled porous media.

A. Microscale modeling of evaporation from hydraulically coupled capillaries of different sizes

Evaporation-induced capillary flow in a porous medium is dominated by two characteristic sizes expressed as equivalent capillary pressures. First is the air-entry pressure defined by the largest drainable pore size (denoted by the index L for large) which is also the capillary pressure at the drying front. The second is defined by the capillary pressure where hydraulic continuity between drying front and evaporating surface is interrupted (denoted by index S for small). When liquid connections break, evaporation becomes diffusion limited and the second stage of drying begins.

Two capillaries representing largest and smallest pore sizes in fine and coarse porous media are shown in Figs. 2(a) and 2(b). The air-entry pressures h_b for the two media are defined by the capillary radii c_L and f_L (with c for coarse and f for fine, respectively). Smallest drainable pore sizes (or

pressures sustaining continuous thick liquid films) are characterized by capillary radii c_S and f_S. The corresponding capillary pressure heads are denoted as $h^c_{\min}$ and $h^f_{\min}$ for coarse and fine materials, respectively.

As in case of homogeneous material, the heterogeneous porous medium containing a distinct vertical textural contrast is represented by a pair of hydraulically coupled capillaries with each capillary representing a characteristic domain of one material [Figs. 2(c) and 2(d)]. To determine the air entrance in fine material, each capillary represents the largest pores of a medium. Air invades the coarse-textured domain through a pore or large capillary of radius c_L and into the fine-textured domain via f_L. Air invades the initially liquid filled and hydraulically coupled capillaries when interface curvature equals the radius of the large capillary c_L. The subsequent penetration of the interface mimics a receding drying front into the coarse-textured domain. Note also that the fixed curvature in the large capillary determines a constant water pressure behind the receding meniscus and capillary gradient inducing flow toward the small capillary with radius f_L. The maximum extent of capillary driving force before air enters the fine medium is determined by the difference in air-entry values between small and large capillaries expressed as capillary pressure head Δh_{cap} (dimension of length),

$$\Delta h_{cap} = \frac{2\sigma}{\rho g}\left(\frac{1}{f_L} - \frac{1}{c_L}\right), \tag{1}$$

with g as acceleration due to gravity, σ as surface tension, and ρ as water density. For vertically oriented capillaries with negligible viscous losses, the magnitude of the capillary driving force (expressed as length Δh_{cap}) adjusts to overcome the gravitational head difference Δh_G between the meniscus in the large capillary and the evaporating surface at the top of small capillary. The maximum length (drying front depth) between menisci in large and small capillaries for which capillarity driving force overcomes gravity is a characteristic of the porous medium defined by the pore sizes and is denoted as gravity length $L_G = \Delta h_G = \Delta h_{cap}$. The maximum depth of the meniscus (drying front) in the large capillary before air enters the fine material is shown in Fig. 2(c).

Capillary-flow required for sustaining stage-1 drying rate persists even while drying front recedes into the fine domain [Fig. 2(d)] with driving capillary pressure difference between drying front in the coarse domain (meniscus in c_L) and the surface of the saturated capillary with radius f_S expressed as follows:

$$\Delta h_{cap} = \frac{2\sigma}{\rho g}\left(\frac{1}{f_S} - \frac{1}{c_L}\right). \tag{2}$$

Hence, in the absence of significant viscous losses, the maximum extent of capillary driving force Δh_{cap} equals the gravitational head difference Δh_G between the meniscus in the largest capillary and the surface. The gravitational head difference equals the drying front depth $L_G = \Delta h_G = \Delta h_{cap}$. In Fig. 2 the front depth L_G for homogeneous and heterogeneous media is shown.

The limitation of liquid flow in capillary by viscous limitations was analyzed in [15] and can be expressed as a characteristic viscous length L_V [10] as discussed explicitly in the forthcoming section for the macroscale.

B. Macroscopic description of evaporation from texturally different and hydraulically coupled domains

Extension of the concept of interacting cylindrical capillaries to real porous media (macroscopic scale) requires introduction of media hydraulic properties, in particular, the hydraulic conductivity $K(h)$ and water content $\theta(h)$ as functions of capillary pressure h (in the following we use the absolute value of capillary pressure).

1. First characteristic length of capillary coupling defining air entry in fine medium

Increasing capillary pressure close to water saturation may not result in noticeable changes in saturation until a critical pressure known as air-entry value h_b is attained [16], where subsequent increase in capillary pressure results in significant drainage and reduction in water content. A similar process occurs during evaporation where propagation of the drying front is associated with menisci exceeding air-entry value followed by air invasion along the front. For coupled domains of coarse and fine porous media, air invades first the domain with lower air-entry value, namely, the coarse-textured domain with air-entry value h^c_b. The fine-textured domain remains saturated until water pressure at the surface reaches the fine-domain air-entry value h^f_b. During evaporation, water flows from coarse-textured domain to the fine-textured surface according to driving capillary pressure gradient of

$$\Delta h_{cap} = h^f_b - h^c_b. \tag{3}$$

The air-entry values and hence the driving capillary pressure difference can be determined experimentally as discussed in Secs. III and IV. As long as the pressure at the surface is less than the critical capillary pressure $h^c_{\min}$ of the coarse, water flow along continuous liquid films in the partially dry coarse region is possible in addition to water flow from coarse to the fine region. The partition between film flow in the coarse and saturated flow in fine material depends on the hydraulic resistances in the two regions.

2. Second characteristic length of capillary coupling defining end of "stage-1" evaporation

Although the region above a receding drying front grows, the drying front remains hydraulically connected with evaporating surface as evidenced by constancy of high evaporation rate during stage 1. Lehmann *et al.* [10] have shown that drying front depth at end of stage 1 could be predicted from macroscopic hydraulic properties of the porous medium (e.g., relationship between liquid saturation and capillary pressure). They used the parametric model of Van Genuchten [17] to quantify the saturation-capillary pressure relationship (also denoted as soil water characteristic or water retention curve),

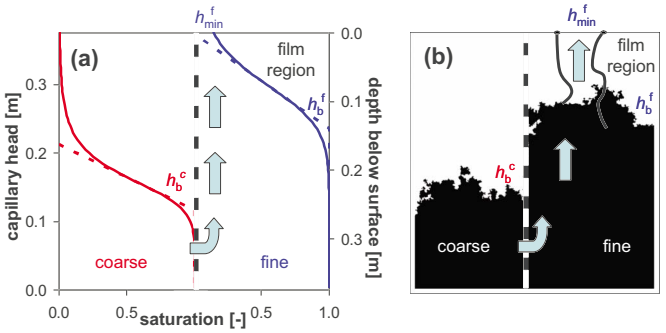

FIG. 3. (Color online) Maximum driving capillary pressure gradient for hydraulically coupled porous media. (a) Water content distribution below the surface at end of stage 1 deduced from the water retention function. The water retention curves (and the corresponding linearization—dashed line) were determined for the two sand media used in the series of laboratory experiments presented in Sec. III. (b) Dye distribution at end of stage 1 with drying fronts in coarse and fine parts. The pressures at the front are equal to the corresponding air-entry values. Saturated regions are shown in black and partially air-filled zones are white. The black lines in the fine indicate continuous liquid structures denoted as "thick films" that sustain liquid flow. Water flow (arrows) is driven by capillary pressure difference between $h^f_{\min}$ (head close to residual saturation for fine material) at the surface and the air-entry value h^c_b at the front of the coarse material.

$$\Theta = \frac{\theta(h) - \theta_{res}}{\phi - \theta_{res}} = [1 + (\alpha h)^n]^{-(1-1/n)}, \tag{4}$$

with effective saturation Θ, volumetric water content $\theta(h)$ for a pressure head h, θ_{res} as the residual water content (where liquid phase becomes fragmented), ϕ as the porosity that equals saturated water content, α as a characteristic inverse pressure head, and the parameter n attributed to pore size distribution. Lehmann *et al.* [10] linearized the saturation pressure relationship to determine air-entry value h_b and capillary pressure close to residual saturation $h_{\min}$.

For hydraulically coupled and texturally different domains, liquid connectivity between the drying front in the coarse domain and the partially wet surface of the fine domain persists until the pressure at the evaporation surface in the fine domain equals $h^f_{\min}$ and the liquid films in the fine region become disconnected. The maximum driving capillary pressure at end of stage 1 is thus

$$\Delta h_{cap} = h^f_{\min} - h^c_b. \tag{5}$$

In Fig. 3 the effect of the hydraulic coupling on the maximum capillary pressure gradient and drying front depth in the coarse material is shown.

3. Viscous losses for upward flow

Flux density through a porous medium is linked to viscous dissipation by Darcy's law (or Buckingham-Darcy for unsaturated conditions). Prior to air entry into the fine-textured domain, flow is controlled (macroscopically) by saturated hydraulic conductivity of the fine medium K^f_s. Following air entry, the unsaturated hydraulic conductivity function $K^f_u(h)$ determines the ensuing flow and viscous dissipation. According to Fig. 3, upward (vertical) water flow in the fine domain is saturated between h^c_b and h^f_b and unsaturated above the drying front for capillary pressure heads $h > h^f_b$. The unsaturated conductivity $K^f_u(h)$ affects viscous dissipation in the film region and limits the characteristic length and front depth. To combine viscous effects in both the saturated and unsaturated fine material we tested different averaging methods and parametrizations and we quantified the effective hydraulic conductivity K^f for the fine material as follows:

$$K^f = \frac{h^f_b - h^c_b}{h^f_{\min} - h^c_b} K^f_s + \frac{1}{h^f_{\min} - h^c_b} \int_{h^f_b}^{h^f_{\min}} K^f_u(h) dh, \tag{6a}$$

$$K^f_u(h) = K^f_s [1 + (\alpha h)^n]^{-(1-1/n)\tau} \left\{ -1 + \left[1 - \frac{1}{1 + (\alpha h)^n} \right]^{1-1/n} \right\}^2, \tag{6b}$$

with the hydraulic conductivity model of van Genuchten [17] and Mualem [18]. The unsaturated hydraulic conductivity $K(h)$ contains an additional parameter τ related to flow path geometry and connectivity and is generally set to 0.5 [17,18].

Stage 1 of evaporation ends when the sum of viscous dissipation expressed as head loss Δh_V in the fine medium and gravitational head difference Δh_G between the evaporating surface and drying front depth in the coarse domain balances the driving capillary pressure difference Δh_{cap}. We start the analysis with the first characteristic length of coupling determining the front depth in coarse material at air entrance into the fine-textured porous medium. First, we neglect the effect of gravity (assuming horizontal arrangement of the soil) focusing on the limitations by viscous effects. The driving capillary pressure equals the differences in the air-entry values $h^f_b - h^c_b$ and is compensated by viscous losses of water flow expressed according to Darcy's law,

$$q = \frac{e_0}{\phi_f} = K^f_s \frac{\Delta h_V}{L_V} \Rightarrow \Delta h_V = \Delta h_{cap} = \frac{1}{K^f_s} \frac{e_0}{\phi_f} L_V \Rightarrow L_V = \Delta h_{cap} \frac{K^f_s \phi_f}{e_0}, \tag{7}$$

with the fraction of the fine-textured medium ϕ_f, the saturated hydraulic conductivity of the fine K^f_s, and a length characteristic for viscous losses expressed as viscous length L_V. By combining viscous and gravitational head losses, a characteristic length L_C just prior to air entry into the fine medium can be computed,

$$\Delta h_{cap} = h^f_b - h^c_b = \Delta h_G + \Delta h_V = L_C \left(1 + \frac{e_0}{\phi_f K^f_s} \right) \to L_C = \frac{\Delta h_{cap}}{1 + \frac{e_0}{\phi_f K^f_s}} = \frac{L_G}{1 + \frac{L_G}{L_V}}. \tag{8}$$

Equation (8) shows that the evaporative characteristic length for porous media with very large hydraulic conductivity (i.e., large viscous length) is determined primarily by the gravitational length.

Frequently the importance of gravitational, viscous, and capillary forces is expressed by dimensionless capillary and bond numbers, denoting the ratio of viscosity or gravity with capillary forces. The definitions of both bond and capillary numbers typically contain a single characteristic pore size which is not directly applicable for determination of characteristic length for drying processes that are driven by a difference of pore sizes. Nevertheless, dividing capillary with bond numbers (by choosing the definitions given in [19]), we can express the ratio between viscous and gravitational length as

$$\frac{\mathrm{Ca}}{\mathrm{Bo}} = \frac{(\eta/\sigma)(e_0/\phi_f)(r^2/\kappa^f)}{r^2(g\rho/\sigma)} = \frac{\eta(e_0/\phi_f)}{\kappa^f g\rho} = \frac{e_0/\phi_f}{K_s^f} = \frac{L_G}{L_V} \Rightarrow L_C = \frac{L_G}{1+\frac{\mathrm{Ca}}{\mathrm{Bo}}}, \tag{9}$$

with capillary number (Ca) and bond number (Bo), representative pore radius r, dynamic viscosity η, and permeability of the fine medium κ^f that is equal to $K_s^f \eta \rho^{-1} g^{-1}$. For small ratio of capillary and bond number viscous effects are small and the resulting characteristic length is close to the gravitational length defined by the width of the hydraulically connected pore size distribution.

For the second characteristic length of coupling defining the end of stage 1, the driving capillary pressure difference is enhanced. The capillary pressure head at the fine-textured surface exceeds the air-entry value and a drying front recedes into the fine-textured material as well. Water flows from the drying front in the coarse toward the surface until the pressure head reaches a value of $h^f_{\min}$. To quantify the viscous dissipation and the characteristic length for end of stage 1, the hydraulic conductivity according to Eq. (6a) must be taken into account. The resulting characteristic length is thus

$$\Delta h_{cap} = h^f_{\min} - h^c_b = \Delta h_G + \Delta h_V = L_C\left(1+\frac{e_0}{\phi_f K^f}\right) \rightarrow L_C = \frac{\Delta h_{cap}}{1+\frac{e_0}{\phi_f K^f}}. \tag{10}$$

Equations (8) and (10) are different with respect to the driving capillary pressure difference and the hydraulic conductivity for the fine. Note that a characteristic front depth could be determined for any driving capillary pressure difference $(h-h^c_b)$ with $h^c_b < h < h^f_{\min}$ but for simplicity we use Eq. (10) as estimate for the characteristic depth at end of stage 1.

Front depth and mass loss in coarse domain are expected to be larger in the heterogeneous (coupled) media compared to uniform coarse porous material due to the enhanced differences in capillary pressure. The ratio of characteristic lengths with and without evaporation-induced hydraulic coupling is enhanced (>1) if the following condition is fulfilled:

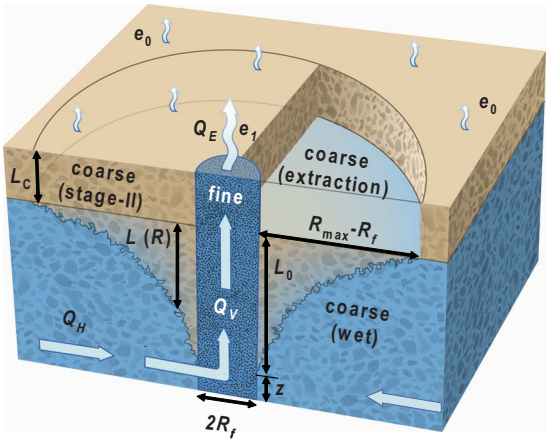

FIG. 4. (Color online) Definition sketch for water extraction from coarse supplying water for evaporation from the fine-textured inclusion surface. Initially, the entire surface evaporates at a rate e_0 until the drying front in coarse reaches its own evaporative characteristic depth L_C. Subsequently, water evaporates only from the fine-textured surface at higher rate e_1 to compensate for the reduced evaporating surface (assuming constant energy input). Water is thus extracted from saturated coarse region to supply evaporation from fine-textured inclusion of radius R_f resulting in a receding interface between saturated and partially unsaturated coarse materials. The horizontal flow Q_H in the coarse (concentrated in a layer of thickness z) matches the vertical flow in fine material Q_V and the evaporative flux from fine-textured surface Q_E. The front depth $L(R)$ below L_C depends on viscous losses associated with horizontal flow. No water is extracted from distances larger than $R_{\max}$ due to limiting viscous losses. The maximum front depth L_0 at the interface is a characteristic length determined by viscous losses in the fine material and the driving capillary pressure difference.

$$\frac{h^f_{\min}-h^c_b}{1+\frac{e_0}{\phi_f K^f}} > \frac{h^c_{\min}-h^c_b}{1+\frac{e_0}{K^c_u}} \rightarrow \frac{h^f_{\min}-h^c_b}{h^c_{\min}-h^c_b} > \frac{1+\frac{e_0}{\phi_f K^f}}{1+\frac{e_0}{K^c_u}}, \tag{11}$$

with the unsaturated hydraulic conductivity of the coarse sand K^c_u. For a small fine-textured fraction ϕ_f and small hydraulic conductivity of the fine K^f, the ratio between capillary pressure difference with and without coupling must be large to enhance evaporative losses.

C. Capillary coupling for heterogeneous system with fine-textured inclusion at larger scales

Thus far, we have considered viscous losses associated with vertical flows through the fine domain only, however, in natural systems of considerable horizontal extent, horizontal flows from coarse-textured domains to fine-textured inclusions and associated head losses might be important for real evaporative losses as well and must be treated in higher spatial dimensions including lateral flow. Here, we characterize evaporation from a system consisting of vertical cylindrical fine-textured inclusion of diameter $2R_f$ embedded in coarse medium of unlimited lateral extent (see Fig. 4). Following a period where the initial evaporation rate e_0 is uniform across

the whole surface (representing ambient atmospheric demand or energy input), the drying front in the coarse domain reaches its own characteristic length and changes evaporation from capillary-driven flow to diffusion controlled evaporation.

The characteristic depth of the coarse sand L_C equals

$$\Delta h_{cap} = h^c_{\min} - h^c_b = \Delta h_G + \Delta h_V = L_C + \frac{e_0}{K^c_u} L_C \rightarrow L_C = \frac{h^c_{\min} - h^c_b}{1 + \frac{e_0}{K^c_u}} \tag{12}$$

by expressing the head loss Δh_V related to an evaporation rate of e_0 using the law of Buckingham-Darcy with unsaturated hydraulic conductivity of the coarse sand K^c_u.

Subsequently, we expect capillary-driven lateral water flow from the coarse to the fine-textured surface that may be limited by viscous effects. Several assumptions could be made regarding the dynamics of evaporation flux from the fine-textured domain and the water flow from coarse to fine medium. For the evaporation flux we have chosen an assumption consistent with small-scale experimental results (presented in Sec. III) where the reduced evaporating surface is compensated by enhancing drying rate at the fine-textured surface from e_0 to e_1 to maintain constant areal average evaporation (such compensation might reflect constant energy input for evaporation). Regarding the water flow from coarse to fine domain driven by capillary pressure difference Δh_{cap} between air-entry value of the coarse h^c_b and minimum capillary pressure in the fine $h^f_{\min}$, we neglect the vertical flow component in the coarse medium. In ground water flow this simplification is known as Dupuit-Forchheimer approximation [20] or vertical flow equilibrium [21] and is valid for a large ratio between lateral and vertical flow distances.

In course of water flow from coarse to fine, water is extracted from the coarse material and the interface between saturated and unsaturated regions in the coarse moves downward. To supply water from coarse to evaporating fine-textured surface, the driving capillary pressure gradient must be larger than the sum of gravitational head difference Δh_G and the viscous head losses related to horizontal and vertical flows, Δh_H and Δh_V, respectively. The gravitational head difference between the position of the front and the surface Δh_G equals the sum of characteristic front depth of the coarse L_C and a depth $L(R)$ depending on the radial distance of the position from where water is extracted. The gravitational head Δh_G and the viscous losses Δh_H due to horizontal flow are a function of radial distance R from the center of fine inclusion. The balance between driving capillary pressure gradient and counteracting gravitational and viscous effects as a function of distance R equals

$$\begin{aligned} \Delta h_{cap} &= h^f_{\min} - h^c_b = \Delta h_G(R) + \Delta h_H(R) + \Delta h_V \\ &= L_C + L(R) + \Delta h_H(R) + \Delta h_V, \end{aligned} \tag{13}$$

with the characteristic length of coarse material L_C according to Eq. (12).

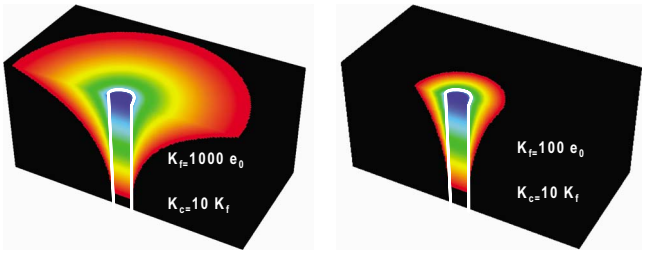

FIG. 5. (Color online) Water extraction from coarse-textured background material through evaporation from surface of a fine-textured inclusion. The white lines indicate the boundary of the fine inclusion. The colors (gray values) depend on the applied capillary pressure difference between the pressure at the top of the fine and the air-entry value of the coarse material (increasing radial distance with increasing pressure difference). The saturated hydraulic conductivities K are given with indices f and c for fine and coarse materials, respectively. With reduced hydraulic conductivity of the inclusion medium, the radius of extraction diminishes.

Viscous effects related to horizontal water flow increase with distance from the fine-textured inclusion. For a maximum radius $R_{\max}$ the viscous dissipation becomes sufficiently large such that no flow is taking place beyond this distance and the drying front depth remains at the characteristic length of coarse medium. We may consider the initial volumetric evaporative flux Q_E from a region of radius $R_{\max}$ as equal to $R^2_{\max}\pi e_0$. The same volumetric flow must be sustained by evaporation from fine-textured inclusion according to

$$R^2_f \pi e_1 = R^2_{\max} \pi e_0 \rightarrow e_1 = e_0 \frac{R^2_{\max}}{R^2_f}. \tag{14}$$

The water evaporating from the fine-textured surface is replaced by water extracted from the coarse sand and the horizontal flow Q_H equals Q_E. At a radial distance R water flows through a cross section of perimeter $2\pi R$ and depth z that will be determined below. The flow balance for radial distance R equals

$$Q_E = Q_H = R^2_f \pi e_1 = 2\pi R z q(R) = 2\pi R z \; K^c_s \frac{dh_H}{dR} \tag{15}$$

with the water flux $q(R)$ as a function of radial distance, the water saturated conductivity of the coarse K^c_s, and the head difference dh_H related to flow across an infinitesimal distance dR. By separating the variables h_H and R and integrating from R_f to $R_{\max}$, the total head loss related to viscous flow Δh_H can be determined,

$$\Delta h_H = \int_{R_f}^{R_{\max}} \frac{e_1 R^2_f}{2 z K^c_s} \frac{dR}{R} = \frac{e_0 R^2_{\max} (\ln[R_{\max}] - \ln[R_f])}{2 z K^c_s}. \tag{16}$$

The result for Δh_H is analogous to the computation of the head loss for confined pumping wells [22,23], here with confinement according to minimizing the viscous components of

water flow as determined below. In this derivation, the vertical flow component in the coarse-textured medium is neglected. This simplification is valid when the ratio between lateral and vertical flow distances is larger than 10 [21] or 5 [20]. As an estimate we choose the ratio between the radial distance $R_{\max}-R_f$ and L_0 (maximum depth of front at the interface between coarse and fine below the characteristic depth of the coarse). As shown in numerical experiments presented in Sec. V this assumption is valid for the analyzed media.

At the interface between coarse and fine materials, the front between saturated and unsaturated regions is at a depth L_0 below L_C. To determine the viscous dissipation in course of vertical flow in the fine inclusion we have to take into account that water flows from a depth z below L_0. The viscous losses and depth L_0 are computed according to the equation for Darcy flow,

$$e_1 = K^f \frac{\Delta h_V}{(L_C + L_0 + z)} \rightarrow \Delta h_V = \frac{e_1}{K^f}(L_C + L_0 + z), \quad (17a)$$

$$\Delta h_{cap} = \Delta h_V + \Delta h_G = (L_C + L_0 + z)\left(1 + \frac{e_1}{K^f}\right)$$

$$\rightarrow L_0 = \frac{h_{\text{cap}}}{\left(1 + \frac{e_1}{K^f}\right)} - L_C - z, \quad (17b)$$

with the average hydraulic conductivity of the fine-textured medium K^f determined by Eq. (6). The thickness of the layer z is chosen to minimize the viscous head loss caused by the horizontal and vertical liquid flows. It can be deduced from solving the derivative of the sum of Δh_V and Δh_H given in Eqs. (16) and (17) as a function of z for zero with z equals

$$z = \sqrt{\frac{(K^f R_f^2 + e_0 R_{\max}^2)(\ln[R_{\max}] - \ln[R_f])}{2K_s^c}}. \quad (18)$$

To determine the maximum distance $R_{\max}$ from the center of the radial inclusion expression from Eqs. (12) and (16)–(18) must be inserted in Eq. (13),

$$\frac{(h_{\min}^f - h_b^c)K^f R_f^2}{K^f R_f^2 + e_0 R_{\max}^2} = \frac{h_{\min}^c - h_b^c}{1 + \frac{e_0}{K_u^c}} + \frac{e_0 R_{\max}^2 (\ln[R_{\max}] - \ln[R_f])}{(\sqrt{2K_s^c (K^f R_f^2 + e_0 R_{\max}^2)(\ln[R_{\max}] - \ln[R_f])})}. \quad (19)$$

The value for $R_{\max}$ was determined numerically. For a given maximum distance $R_{\max}$, the front depth $L(R)$ below L_C can be determined,

$$L(R) = \frac{(h_{\min}^f - h_b^c)K^f R_f^2}{K^f R_f^2 + e_0 R_{\max}^2} - \frac{h_{\min}^c - h_b^c}{1 + \frac{e_0}{K_u^c}} - \frac{e_0 R_{\max}^2 (\ln[R] - \ln[R_f])}{(\sqrt{2zK_s^c (K^f R_f^2 + e_0 R_{\max}^2)(\ln[R_{\max}] - \ln[R_f])})}. \quad (20)$$

An example of the front depth $L(R)$ below the characteristic depth of the coarse domain and the water extraction in three dimensions by capillary coupling is shown in Fig. 5. The figure shows nonlinear decrease in drying (or extraction) front depth as a function of radial distance. Increasing hydraulic conductivity of fine (or coarse) domains reduces viscous losses and water may be extracted from larger radial distances.

To compute the extracted volume, we assume at end of stage 1 of the coarse a linear water content profile between L_C (complete water saturation with water content equals porosity ϕ) and the surface with residual water content θ_{res}. Due to the hydraulic coupling, the front between saturated and partially water filled zones in the coarse decreases to a larger depth $[L_C+L(R)]$. Between the surface and depth $L(R)$ the water content equals θ_{res} and a water column of height $L(R)(\phi-\theta_{\text{res}})$ was extracted by water flow from coarse to fine-textured surface. The volume V of extracted water equals

$$V = (\phi - \theta_{\text{res}}) \int_{\gamma=0}^{\gamma=2\pi} \int_{R=R_f}^{R=R_{\max}} RL(R) dR d\gamma, \quad (21)$$

with the angle γ ranging from 0 to 2π.

III. EXPERIMENTAL CONSIDERATIONS

A. Laboratory experiments

Experimental studies on effects of hydraulic coupling on evaporation were carried out with two quartz sand media denoted as "fine sand" (particle sizes of 0.1–0.5 mm) and "coarse sand" (0.3–0.9 mm), respectively. The hydraulic properties of these sand media were analyzed with respect to their water retention and saturated hydraulic conductivity [10]. To compare measurements of evaporative mass loss with drying front position we used glass Hele-Shaw cells of 260 mm height and 10 mm thickness. To enhance visibility of fluid distribution, we used degassed dye solution (brilliant blue, 0.5–1.0 g l^{-1}). In a first experiment (presented in Fig. 1) a Hele-Shaw cell of 200 mm width was subdivided into

four compartments with three filled with single material (fine and coarse sands, glass beads) and a fourth cell with hydraulically coupled coarse and fine sands (the glass bead cell is not analyzed in this paper). An image was acquired every hour to monitor the position of the drying front.

All other drying experiments were carried out with Hele-Shaw cells of 75 mm width. Four columns with a vertical contrast were packed with fine and coarse sands with fractions of fine sand, 75%, 50%, 25%, and 8%. Two columns filled with a single porous medium (coarse or fine) were used for comparison with hydraulically coupled columns under similar evaporative conditions. To pack a column with vertical contrast, a thin aluminum bar of 10 mm width was inserted in the Hele-Shaw cell. At both sides of the aluminum bar sand particles were filled in. To obtain completely saturated initial conditions, the sand particles were dropped into the liquid with the water table always above the sand surface. With increasing level of the sand packing the aluminum bar was lifted carefully, with the bottom of the bar at about 10–20 mm below sand surface. Each of the Hele-Shaw cells was mounted on a digital balance for continuous monitoring of evaporative mass losses. Air humidity and ambient temperature were monitored using computer-controlled sensor (Hygrowin, Rotronic, Switzerland) recording measured values once per minute. In several experiments fans were installed to enhance potential drying rates. To determine the potential evaporation rate, the mass loss from a water filled column connected to a Mariotte bottle (to sustain constant water level in the cell) mounted on a balance was monitored as well. The fluid distribution marked by the blue dye was imaged once or twice every hour with digital camera.

B. Neutron transmission measurements

To deduce water and air content above the drying front, series of experiments were performed at the Swiss spallation neutron source SINQ [Paul Scherrer Institute (PSI), in Villigen Switzerland] with neutron radiography imaging at beamline NEUTRA [24]. Neutrons are attenuated by hydrogen nuclei and are very sensitive to the presence of water. Neutron transmission is a useful technique to measure nondestructively the water content in porous media [25,26] and was applied in a former study on drying front morphology [13]. The attenuation of neutrons passing a Hele-Shaw cell ($260\times75\times10$ mm^3) mounted on a digital balance was measured every 5 min. To optimize the limited beam time at the NEUTRA station, the experiment was carried out under high evaporative demand with a potential drying rate of about 31 mm/day. A detector of size 97×97 mm^2 mapped the incoming neutrons with a resolution of about 0.1 mm. The Hele-Shaw cell was packed such that a vertical contrast was formed with one half filled with fine and the other half filled with coarse sand. To observe the expected flow of the fluid from coarse to fine sand, the bottom of the column was filled with D_2O (heavy water) and only the uppermost 61 mm of the porous medium was filled with H_2O (light water). Due to the neutron in the nucleus of the deuterium atom, the interaction with the neutron beam is different compared to H_2O and the attenuation is tenfold less in case of heavy water. The different attenuations of heavy and light waters make it possible to use heavy water as a tracer and the interface between heavy and normal water could be monitored.

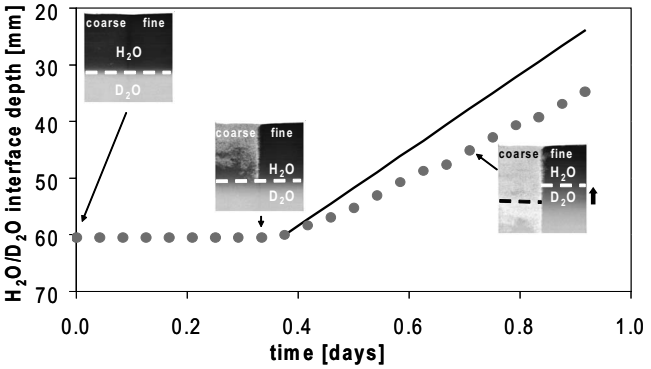

FIG. 6. The position of interface between heavy and normal waters in the fine domain was monitored using neutron radiography to delineate water flow driven by evaporation in hydraulically coupled sand media. Neutron transmission images are inserted to show the motion of the drying front and the H_2O/D_2O interface. Zones saturated with normal water are dark gray and heavy water and partially air-filled regions are indicated by bright values. Air penetrates preferentially the coarse material. When the drying front in the coarse reaches the initial H_2O/D_2O interface at a depth of 61 mm after 0.33 days, the boundary between the two liquids is moving upward in the fine domain due to water extraction from the coarse sand pushing (heavy) water toward the fine-textured surface, a process driven by the capillary pressure difference between the surface of the fine and the drying front in the coarse. The liquid interface moves with a velocity of about 47 mm/day. The black line indicates the drying rate expressed as velocity and corresponds to the expected H_2O/D_2O interface velocity when water is evaporated exclusively from the fine material. The difference between this line and measured velocity is caused by vertical flow in the partially air-filled coarse medium along thick liquid films.

IV. RESULTS

A. Preferential drying front displacement and water flow from coarse to fine medium

Neutron transmission images were used for observing preferential displacement of the drying front into the coarse medium and of lateral flows between the hydraulically coupled domains. We tracked the motion of the H_2O/D_2O interface in fine sand to determine the flow velocity from coarse to fine material. Figure 6 depicts the position of the interface between heavy and light waters as a function of time and shows neutron transmission images for three different time steps. Initially, the interface between the heavy and normal waters is indicated as distinct contrast in 61 mm depth between high (D_2O) and low (H_2O) gray values. During evaporation, air invades the coarse sand domain exclusively and the interface between the two liquids spreads slightly by diffusion. After 0.33 days the drying front in the coarse domain reaches the H_2O/D_2O interface and subsequently upward motion of the interface between the two liquids is apparent in the fine sand domain. The upward motion

of the interface confirms the postulated mechanism of lateral water extraction from the coarse region driven by more negative capillary pressure at the fine-textured surface pulling the liquid interface upward. The heavy water of the coarse sand is pushed into the fine region by capillary pressure difference between the drying front and fine sand surface.

It is interesting to note that the H_2O/D_2O interface remains stationary until the drying front reaches the interface depth, indicating that the lateral exchange so far occurred above the interface location (always taking the shortest path between the two domains). The fine sand remains water saturated until the drying front in the coarse is at depth of about 100 mm after 0.7 days. As shown in Fig. 6, the interface between heavy and light waters starts moving after 0.33 days with a mean velocity of about 47 mm/day. We use this estimated pore water velocity to analyze if pathways in the film region of the coarse region contribute to evaporation from partially dry coarse surface. The deduced pore water velocity in the coarse part corresponds to a flux density of about 20 mm/day (with porosity of 0.42). When scaling by the entire cross sections of both coarse and fine, the flux density equals 10 mm/day and is comparable with measured evaporation rate. Due to decreasing surface water content and thus coupling with the atmosphere, the drying rate decreased from initially 31 to 14 mm/day and was higher than estimated lateral water exchange from coarse to fine sand (of about 10 mm/day). We thus conclude that although lateral water exchange between the domains dominated the process, vertical flow within the partially saturated coarse domain along liquid films was about 4 mm/day at the end of stage 1 evaporation and cannot be neglected. As soon as the pressure at the surface is negative enough to interrupt the films in the coarse domain, water transport in the coarse will be limited by vapor diffusion.

B. First characteristic length of capillary coupling defining air entry in fine medium

During evaporation from hydraulically coupled columns with vertical textural contrast, air phase invades preferentially the coarse sand domain while the fine sand remains completely water saturated. When drying front in coarse domain had reached a depth of about 100 mm, air invades the fine sand as well. Liquid distributions (as marked by dye patterns) in the experimental columns are shown in Fig. 7 for conditions just before air entry into the fine sand. Results clearly show that drying front depth reaches the same depth (at the point of air entry into the fine) irrespective of the fraction of the fine sand domain. The drying front in the coarse sand receded most rapidly in the column with 75% fine fraction and arrived in a depth of 100 mm after less than 2 days. The smaller the fraction of the coarse material, the less water volume was extracted from the coarse domain before the drying front reaches 100 mm depth. Hence, for a constant drying rate e_0, the time for drying front depth of 100 mm decreased with decreasing fraction of coarse sand.

The value of drying front at air entry into fine (about 100 mm) could be understood by analyzing water retention functions of the two materials shown in Fig. 3. From these functions we observe a characteristic air-entry value of $h_b^c = 120$ mm for coarse sand and about $h_b^f = 230$ mm for the fine sand. Liquid flow from coarse to fine material is thus driven by capillary pressure difference $h_b^f - h_b^c$ [see Fig. 2(c)] of 110 mm. This capillary driving force is balanced by gravitational head difference between drying front depth and evaporating surface. Hence a drying front depth of 100 mm is about the value to the driving capillary pressure difference (110 mm) within the experimental accuracy of determining front depth position and air-entry values.

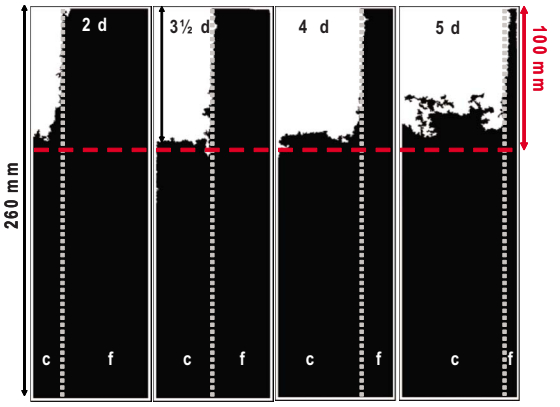

FIG. 7. (Color online) Dye distribution in the four hydraulically coupled columns just before air enters the fine sand area. The dye distribution was classified as water saturated (black) and partially air filled (white). Air enters exclusively the coarse (c) sand until the depth of the drying front is about 100 mm (horizontal dashed line) and is close to the difference of the air-entry values of the two materials. The fraction of the fine (f) sand decreases from the left from 75%, 50%, 25%, and 8% and determines the time (indicated at the top of each column) until the drying front reaches 100 mm depth. The dashed vertical line indicates the position of the interface between the coarse and fine textural domains.

Obviously, the drying front depth in the coarse before air entry into the fine domain was not affected by viscous flow within the fine sand. The drying rate e_0 in the range of 5 mm/day and a minimum fine fraction of 8% resulted in maximum water flux of 62.5 mm/day. With the saturated conductivity of 58.8 m/day for fine sand, the capillary and bond numbers where 6×10^{-7} and 6×10^{-4} with a small ratio Ca/Bo of 1×10^{-3} indicating a minor effect of viscous resistance on characteristic length L_C according to the expression given in Eq. (9).

C. Second characteristic length of capillary coupling defining end of stage-1 evaporation

Even after air entry into the fine sand, the drying fronts in both coarse and fine domains continue to recede with almost no effect on original drying rate. For the hydraulically coupled columns the driving capillary pressure gradient is determined by the difference between largest and smallest hydraulically connected pores ($\Delta h_{cap} = h_{\min}^f - h_b^c$) and is equal to 250 mm for the sands under study. This is similar to column length and the drying front in the coarse sand domain may reach the bottom of the column during stage 1 with little effect on drying rate. As long as the pressure at the surface is

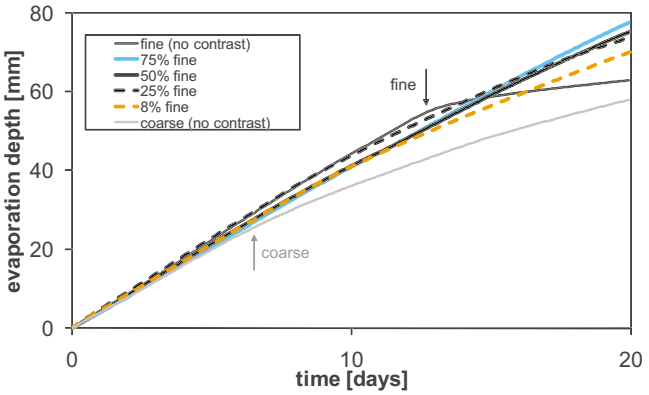

FIG. 8. (Color online) Evaporative losses expressed as equivalent depth (evaporated water volume per column cross-sectional area) shown for four columns with vertical contrast and for the homogeneous fine and coarse sand columns. The arrows mark end of stage 1 evaporation from uniformly-packed columns. In the homogeneous fine sand the evaporation rate drops when the drying front reaches a depth of about 140 mm (evaporation depth of 55 mm) and the hydraulic connections between the front and the surface breaks. For the coarse sand the rate drops at a front depth of about 90 mm (evaporation depth of 25 mm). In the hydraulically coupled columns water flows from the coarse to the surface of the fine medium spanning a distance of the entire column length without significant drop in drying rates.

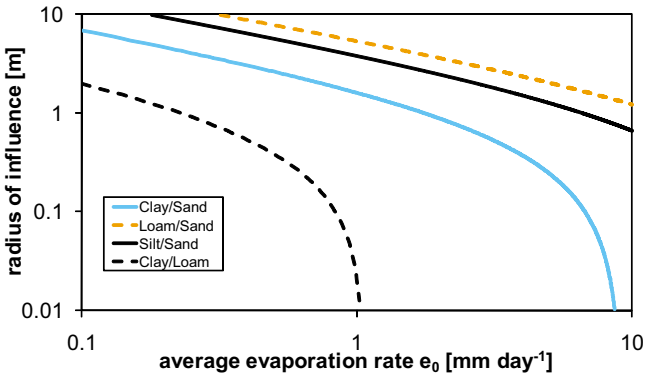

FIG. 9. (Color online) Numerical estimates of range of radial influence of fine-textured inclusion with radius $R_f=1.0$ m for initial drying rates e_0 ranging from 0.1 to 10 mm/day. The radius of influence $(R_{max}-R_f)$ is the maximum radial distance, where the drying front in the coarse domain is equal to its characteristic length and hydraulic coupling between fine and coarse vanishes. For the four coupled textures presented in the figure, sand is the background medium in three cases and loam serves as background for clay inclusion.

less negative than the minimum pressure h^f_{min}, thick liquid films in the fine material remains continuous and water is extracted from the drying front in the coarse and flows first through the water saturated region of the fine and then along films in the partially water saturated fine region.

The drying rates of four columns with vertical textural interfaces between fine and coarse sands were compared with drying behavior of homogeneous columns filled with either coarse or fine sand. As shown in Fig. 8, cumulative mass loss is higher for the hydraulically coupled columns as compared with the homogeneous fine or coarse sand material. The drop in drying rate for the homogeneous fine medium is a consequence of attaining its characteristic length $(h^f_{min}-h^f_b)$ of about 140 mm. The transition occurred after evaporation depth (mass loss per cross section) of about 55 mm. The drop of drying rate at end of stage 1 for the homogeneous coarse material is less distinct and happened after evaporation depth of about 25 mm.

For hydraulically coupled columns, the driving capillary pressure gradient of about $h^f_{min}-h^c_b=250$ mm supports drying front displacement in the coarse sand to the bottom of the column before end of stage 1. Even for the smallest fractions (8%) of fine sand domain no transition to stage 2 was observed indicating that viscous losses are relatively minor. Calculations of flow rates for initial drying rate e_0 of 5 mm/day indicate that water flux through 8% fine sand domain fraction was about 62 mm/day (assuming all water was evaporated exclusively from the fine surface). Even for such a high local evaporative flux, the value is small as compared with the intrinsic value of saturated hydraulic conductivity K_s of 58.8 m/day indicating a ratio K_s/e_0 of about 1000 (hence negligible viscous losses).

V. SPATIAL EXTENT OF HYDRAULIC COUPLING

To generalize experimental findings presented in Sec. IV and the potential role of viscous dissipation in larger field scale systems, we carried out numerical experiments in three dimensions. The hydraulic functions of various soil classes were chosen according to Carsel and Parrish [27] that determined the parameters of the van Genuchten [17] model and the saturated hydraulic conductivity for 12 soil classes.

A. Radius of influence for evaporation from fine-textured inclusions

Lateral flow between coarse- and fine-textured domains to supply evaporation from a fine-textured surface coupled with the atmosphere is limited by viscous resistance to flow through both coarse and fine domains. Combinations of soils with different textures designated as "clay," "loam," "silt," and "sand" were analyzed using hydraulic parameters reported by Carsel and Parrish [27]. For comparison and simplicity we employed axial symmetry with a fixed radius of fine-textured inclusion of 1 m and considered initial evaporation rates from wet surfaces in the range of 0.1–10 mm/day (range of evaporation from terrestrial surfaces). The maximum lateral extent of evaporative water extraction equals $R_{max}-R_f$, with R_{max} determined from Eq. (19). In computational results summarized in Fig. 9 we assumed that evaporation rate from the fine-textured surface adjusts to accommodate lateral flows. Water extracted from the maximum radial distance R_{max} evaporates from the fine-textured surface at local rate $e_1=R^2_{max}/R^2_f e_0$.

Computations show that despite considerable increase in flux and viscous dissipation, certain combinations of porous media sustain water extraction to distances in excess of 10 m

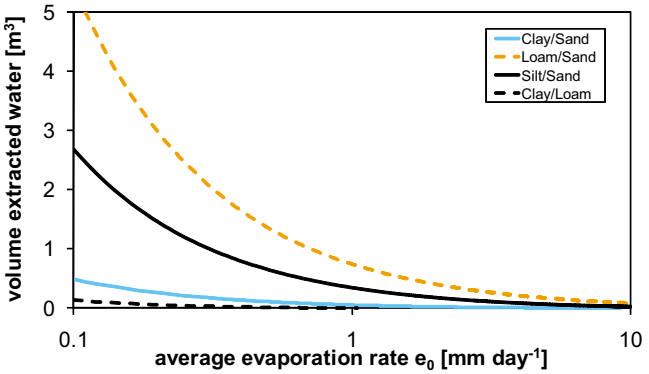

FIG. 10. (Color online) Water volume extracted from coarse sand by evaporation from fine-textured inclusion of radius $R_f = 1.0$ m for initial drying rates e_0 in the range of 0.1–10 mm/day. The volume increases with the hydraulic conductivity of the inclusion material. For clay as inclusion medium, the extracted volume decreases with the conductivity of the background material (which is 30 times larger for sand compared to loam).

(especially for low initial evaporation rates). Viscous limitations become more important for clay inclusions as compared with silt and loam, resulting in limited radius of evaporative water extraction. Simulation results neglect vertical flow component in the coarse medium. This is justified for ratio of lateral flow distance $R_{\max} - R_f$ to vertical flow distance L_0 larger than 5–10 [20,21]. For combination of silt and sand (this ratio is >21), and loam and sand (ratio >25) this criterion is fulfilled. Only in case of clay inclusion the ratio becomes smaller than 5 for average evaporation rates larger than 8.4 mm/day for sand as background material (0.9 mm/day for loam as background material).

The amount of water volume extracted from the coarse domain by evaporation from 1 m radius fine-textured inclusion is depicted in Fig. 10. It is maximal for sand coupled with a loamy inclusion in agreement with the largest spatial extent of hydraulic coupling shown in Fig. 9.

B. Heterogeneity and spatial distribution of fine inclusions

In nature, distinct vertical contrasts between materials of different textures can be caused by wind erosion, termites, worm burrows, sequences of freezing, and thawing or swelling and shrinking. Additionally, vegetation patterns in semiarid regions may affect the spatial distribution of texture due to effects on wind deposition and water erosion, in general with a higher fraction of fine particles deposited at shrub mounds [28]. A different interaction between soil texture and vegetation affected by swelling and shrinking of clay is presented in Fig. 11 with small density of vegetation in patches of loamy texture at the mounds compared to vegetation rich depressions with clay soils [29]. While the loamy mounds (25% clay) have small infiltration capacity due to sealing effects, water can penetrate deeper in cracks of the clay material (55% clay) and along root channels. The spatial distribution of different textural inclusions and the extent of heterogeneity are expected to affect evaporative losses or water extraction by evaporation due to the subterranean hydraulic coupling. For illustration purposes, we selected sand as background soil and loam as inclusion material (mimicking hypothetical scenario of aeolian loam material trapping by desert vegetation [28]). We analyzed three patterns of fine inclusions with a total cross-sectional area of 15%. This value and the radius of 1.2 m for one case of inclusion pattern were deduced from a study on spatial distributions of shrubs [30].

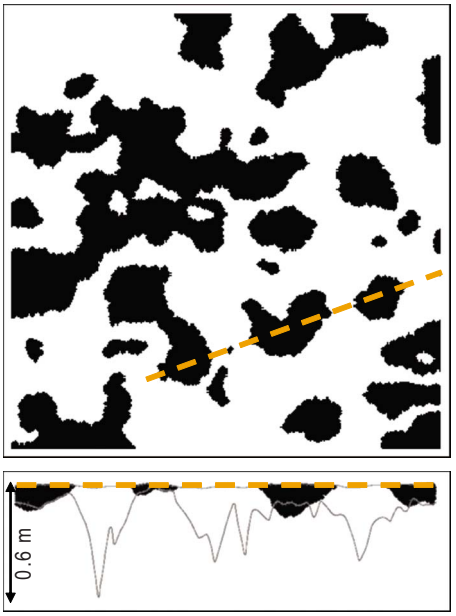

FIG. 11. (Color online) Figure adapted from Warren Wilson and Leigh [29] showing the distribution of loamy patches (black) with less vegetation compared to the clay material (white). Along an 11 m transect shown in orange (dashed bold line), the water front after heavy rainfall was measured (gray solid line in bottom figure) indicating higher water content in clay soil. The patchiness of soil types and vegetations motivates the numerical example shown in Fig. 12.

For a region of 25×25 m^2, 20 structures of 1.2 m in radius were distributed randomly based on the constraint that they do not overlap. This pattern was compared to a single inclusion in the center of the system. In the last case structures with 1/20 of the initial cross section were chosen. The resulting radii in the three patterns were 0.27, 1.2, and 5.46 m, respectively. The water extracted from the coarse medium by evaporation from the fine-textured inclusion was estimated for initial drying rates of 1.0 and 10 mm/day. We assumed that the drying rate of the fine inclusion will be enhanced to compensate the reduction in evaporating surface when the drying front exceeds the characteristic depth of the coarse material. We computed the maximum range $R_{\max}$ of water extraction as a function of drying rate and size of the fine inclusion R_f. For the high drying rate the values for $R_{\max}$ for small, intermediate, and large structures were 0.72, 2.54, and 8.46 m (2.17, 7.32, and 22.21 m for low drying rate). The radius of extraction and the pattern of fine inclusions are shown in Fig. 12.

For the low drying rate water is extracted from the entire domain's cross section in all three cases. For high drying rates the fraction of coarse sand affected by evaporation from

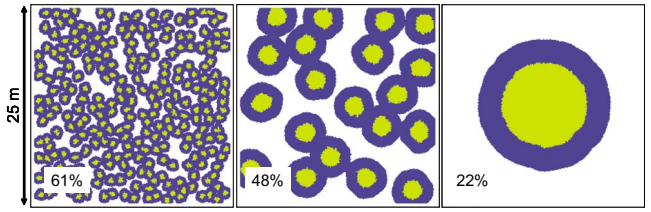

FIG. 12. (Color online). Effect of spatial distribution of fine inclusions on water extraction from background coarse material. In green (bright gray values) the spatial distribution at the surface of fine-textured inclusions is shown where fraction of fine inclusion is fixed at 15% of the surface but the inclusion radius varies from 0.27 (left) to 1.20 (center) and 5.46 m (right). Water extraction under mean evaporation rate of 10 mm/day was computed for sandy background and loamy inclusions [lateral extent of water extraction shown in blue (dark gray)]. The numbers indicate the cross-sectional fraction of the region with evaporative water extraction. Despite the fact that small inclusions can extract water from a larger lateral extent (as indicated by higher fraction), the extracted volume is smaller due to high viscous losses in smaller fine-textured inclusions with increasing flux density.

fine inclusions increases with decreasing structure size (or increasing interfacial length between the two soil textures). For inclusions with smallest radius, water was extracted from 61% of the cross section under the evaporation rate 10 mm/day.

In addition to estimation of cross-sectional area affected by the inclusion, the volume of extracted water was also determined. For each pixel of the image (spatial resolution of 0.1 m) the depth of the front in the coarse and drainable water fraction as a function of the radial distance from the closest inclusion was computed. We found that larger inclusions resulted in larger extracted water volumes. For areal average evaporation rate of 10 m/day, the extracted volumes from the entire domain under study were 1.31, 2.54, and 2.7 m^3 for small, intermediate, and large inclusions. The different volumes can be explained by different shapes of the front depth as a function of radial distance for different inclusion size. With increasing size of the structure R_f the ratio $R_{\max}/R_f$ becomes smaller. For small inclusions the ratio is high indicating a flat and shallow front depth. For large structures the front depth as a function of radius is rather steep reaching higher depth close to the material interface. For large values of R_f the flux density and the hence the viscous dissipation in the fine are small and the front can penetrate deeper. These results highlight the dependency of evaporation behavior on soil and textural heterogeneities and their spatial distributions and link field scale evaporative losses with potential evaporation rates and spatial heterogeneity.

VI. SUMMARY AND CONCLUSIONS

Capillary induced liquid flow from internal drying front to the surface supports high and nearly constant evaporation rates from porous media during stage 1. Gravity and viscous dissipation limit the extent of the partially saturated region between the drying front and evaporating surface. These interactions are conceptualized using pairs of hydraulically coupled capillaries of different sizes. In this study, the concept of coupled capillaries was extended to analyze evaporation from porous media containing a sharp vertical textural contrast. The driving capillary forces typically depending on the width of pore size distribution for a porous medium are enhanced when hydraulic coupling of two texturally different media is considered. Based on theoretical considerations and experimental results we arrive at the following conclusions for evaporation from porous media with sharp vertical contrast:

(i) Drying front forms and propagates preferentially into the coarse-textured medium whereas the fine-textured domain remains water saturated resulting in a remarkably sharp contrast in water contents.

(ii) Air enters into fine material when the drying front depth in the coarse material equals the difference between the air-entry values of the two materials, defining a first characteristic length of coupling (extent of saturated fine region above drying front in the coarse).

(iii) The capillary pressure difference between drying front in the coarse and surface of the fine region results in a horizontal flow component from the coarse to the fine domain.

(iv) Although most evaporation takes place from the fine-textured surface, some evaporation may occur through the coarse surface due to flow along continuous liquid films (and via vapor transport).

(v) Following air entry into fine-textured domain evaporation rate may not be affected and remains at stage 1 as long as hydraulically continuous water films in the fine domain remain uninterrupted, defining a second characteristic length of coupling.

(vi) The maximum extent of liquid pathways connecting drying front in coarse to evaporating surface in fine domain is defined by the width of their drainable pore size distributions deduced from their water retention characteristics.

(vii) Based on numerical experiments, the lateral extent of evaporation-induced water extraction may exceed 10 m thereby could be of significant hydrological and ecological importance.

The findings of this study can be used to construct arrangement of materials and inclusions to control the drying rate. For example, Abu-Zreig *et al.* [31] proposed a method called "evaporation drainage" by inserting fabric columns from where water is evaporating preferentially. Our study reveals that the hydraulic coupling may dominate the evaporation rate from heterogeneous surfaces resulting in larger evaporative losses than would have been predicted from consideration of single porous media properties alone. Results also anticipate heterogeneity of evaporative fluxes at scales similar to near surface soil textural heterogeneity. This patchiness affects thermal signatures used for remote sensing of water and energy balances of heterogeneous evaporating surfaces. Hence, models of water exchange between atmosphere and terrestrial systems must take into account the effect of surface heterogeneity on water extraction from coarse-textured materials.

ACKNOWLEDGMENTS

The authors gratefully acknowledge funding by the Swiss National Science Foundation (SNSF) Project No. 2000021-113676/1. We thank Nima Shokri (ETH Zürich) and Peter Vontobel (PSI-NEUTRA) for their support during neutron imaging experiments. We thank Shmuel Assouline from the Volcani Center (Israel) for his helpful comments on a previous version of the paper and we acknowledge the constructive comments by reviewer and associated editor.

[1] T. M. Shaw, Phys. Rev. Lett. **59**, 1671 (1987).
[2] A. A. Van de Griend and M. Owe, Water Resour. Res. **30**, 181 (1994).
[3] A. G. Yiotis, A. G. Boudouvis, A. K. Stubos, I. N. Tsimpanogiannis, and Y. C. Yortsos, Phys. Rev. E **68**, 037303 (2003).
[4] J. B. Laurindo and M. Prat, Chem. Eng. Sci. **51**, 5171 (1996).
[5] M. Prat and F. Bouleux, Phys. Rev. E **60**, 5647 (1999).
[6] G. W. Scherer, J. Am. Ceram. Soc. **73**, 3 (1990).
[7] I. N. Tsimpanogiannis, Y. C. Yortsos, S. Poulou, N. Kanellopoulos, and A. K. Stubos, Phys. Rev. E **59**, 4353 (1999).
[8] P. Coussot, Eur. Phys. J. B **15**, 557 (2000).
[9] T. Engøy, J. Feder, and T. Jøssang, Phys. Scr. **T38**, 99 (1991).
[10] P. Lehmann, S. Assouline, and D. Or, Phys. Rev. E **77**, 056309 (2008).
[11] S. Suzuki and S. Maeda, J. Chem. Eng. Jpn. **1**, 26 (1968).
[12] E.-U. Schlünder, Chem. Eng. Sci. **43**, 2685 (1988).
[13] N. Shokri, P. Lehmann, P. Vontobel, and D. Or, Water Resour. Res. **44**, W06418 (2008).
[14] O. Krischer, *Die Wissenschaftlichen Grundlagen der Trocknungstechnik* (Springer, Berlin, 1956), p. 237.
[15] T. Metzger and E. Tsotsas, Drying Technol. **23**, 1797 (2005).
[16] R. H. Brooks and A. T. Corey, *Hydrology Paper 3* (Colorado State University, Fort Collins, CO, 1964).
[17] M. Th. Van Genuchten, Soil Sci. Soc. Am. J. **44**, 892 (1980).
[18] Y. Mualem, Water Resour. Res. **12**, 513 (1976).
[19] D. Or, Adv. Water Resour. **31**, 1129 (2008).
[20] N.-O. Kitterød, Water Resour. Res. **40**, W11507 (2004).
[21] Y. C. Yortsos, Transp. Porous Media **18**, 107 (1995).
[22] D. Hillel, *Introduction to Environmental Soil Physics* (Elsevier Science, New York, 2004).
[23] P. Renard, in *Hydraulics of Wells and Well Testing, Encyclopedia of Hydrological Sciences*, edited by M. G. Anderson (Wiley, New York, 2005).
[24] http://neutra.web.psi.ch
[25] J. D. Schaap, P. Lehmann, A. Kaestner, P. Vontobel, R. Hassanein, G. Frei, G. H. de Rooij, E. Lehmann, and H. Flühler, Adv. Water Resour. **31**, 1233 (2008).
[26] S. E. Oswald, M. Menon, A. Carminati, P. Vontobel, E. Lehmann, and R. Schulin, Vadose Zone J. **7**, 1035 (2008).
[27] R. F. Carsel and R. S. Parrish, Water Resour. Res. **24**, 755 (1988).
[28] S. Ravi, P. D' Odorico, and G. S. Okin, Geophys. Res. Lett. **34**, L24S23 (2007).
[29] J. Warren Wilson and J. H. Leigh, J. Ecology **52**, 379 (1964).
[30] I. O. McGlynn and G. S. Okin, Remote Sens. Environ. **101**, 554 (2006).
[31] M. M. Abu-Zreig, Y. Abe, and H. Isoda, Canadian Biosystems Engineering **48**, 1.25 (2006).